Spatial stability and the onset of absolute instability of Batchelor's vortex for high swirl numbers

L. PARRAS AND R. FERNANDEZ-FERIA

Universidad de Málaga, E.T.S. Ingenieros Industriales, Pza. El Ejido, s/n 29013 Málaga, Spain

Batchelor's vortex has been commonly used in the past as a model for aircraft trailing vortices. Using a temporal stability analysis, new viscous unstable modes have been found for the high swirl numbers of interest in actual large-aircraft vortices. We look here for these unstable viscous modes occurring at large swirl numbers ($q > 1.5$), and large Reynolds numbers ($Re > 10^3$), using a spatial stability analysis, thus characterizing the frequencies at which these modes become convectively unstable for different values of q, Re, and for different intensities of the uniform axial flow. We consider both jet-like and wake-like Batchelor's vortices, and are able to analyse the stability for Re as high as 10^8. We also characterize the frequencies and the swirl numbers for the onset of absolute instabilities of these unstable viscous modes for large q.

1. Introduction

We consider here the spatial stability of the so-called *q-vortex*, also called Batchelor's vortex, whose velocity field (U, V, W), in cylindrical polar coordinates (r, θ, z), is given, in dimensionless form (see §2 for more details), by

$$U = 0, \quad V = \frac{q}{r}\left(1 - e^{-r^2}\right), \quad W = W_0 + e^{-r^2}, \tag{1.1}$$

where q is the swirl parameter, and W_0 is a uniform axial flow, which can be positive (jet-like vortex), negative (wake-like vortex), or zero. All the velocities are made dimensionless with a characteristic axial velocity W_c that accounts for the exponential part of the axial flow in (1.1). This model vortex is a parallel-flow approximation of the original Batchelor's (1964) vortex, and has been traditionally used as a simple model for trailing vortices with axial flow (see, e.g. Lessen, Singh & Paillet; Mayer & Powell 1992).

The temporal stability of the q-vortex (1.1) was first considered by Lessen and colleagues, both from an inviscid point of view (Lessen *et al.* 1974), and taking into account the effects of viscosity (Lessen & Paillet 1974). In these works, as in all the temporal stability results of later works commented on below, the uniform advection velocity W_0 was set to zero without loss of generality, for this parameter is not relevant in the temporal stability problem because of Galilean invariance. These authors found that (1.1) was unstable to non-axisymmetric counter-rotating perturbations ($n < 0$) in a wide range of the swirl number q and the Reynolds number Re (see §2 for its exact definition). In fact, Lessen *et al.* (1974) and Lessen & Paillet (1974) only reported inertial instabilities, finding that the widest unstable range of swirl numbers is $0 \leqslant q \leqslant q_{crit} \simeq 1.5$, corresponding to $Re \to \infty$ for the azimuthal

wavenumber $n = -1$. These results were later refined numerically by Duck & Foster (1980), and generalized asymptotically for $|n| \gg 1$ by Leibovich & Stewartson (1983), Stewartson & Capell (1985), and Stewartson & Leibovich (1987).

Purely viscous modes corresponding to azimuthal wavenumbers $n = 0$ and $n = +1$ were found by Khorrami (1991a) and by Duck & Khorrami (1992). These modes occur for $q < 1.3$, and their growth rates are always several orders of magnitude smaller than those of the corresponding inertial modes. A detailed characterization of the temporal stability of the q-vortex in the (Re, q)-parameter plane, including all the inviscid and viscous modes found previously and some new ones (particularly for $n \geqslant 0$), was made by Mayer & Powell (1992) (see also the review by Ash & Khorrami 1995).

Viscous instabilities for large swirl numbers ($q > 1.5$) and large Reynolds numbers ($Re > 10^3$) were found asymptotically by Stewartson & Brown (1985). Fabre & Jacquin (2004) made a detailed characterization of these large swirl number viscous instabilities by solving numerically the temporal stability problem. These instabilities were not found previously, particularly in the detailed work of Mayer & Powell (1992), because the unstable perturbations are centre modes which are concentrated along the vortex axis, and they can only be found with a highly accurate spectral method such as that used by Fabre & Jacquin. These authors were able to map the unstable region up to $Re \approx 10^6$ and $q \approx 7$. These unstable modes are related to the family of viscous modes found by Stewartson, Ng & Brown (1988) for a swirling pipe Poiseuille flow.

A spatial stability analysis of the q-vortex, characterizing the unstable regions and the onset of absolute instabilities in the (Re, q)-parameter plane for all possible values of W_0, was undertaken by Olendraru & Sellier (2002). Although these authors also found unstable modes for large q (up to $q \approx 3$), they did not explore systematically these viscous modes for large q. Therefore, the main objective of this work is to perform such a systematic characterization of viscous unstable modes for large values of the swirl parameter and for large Reynolds numbers from a spatial stability analysis. Our numerical technique allows us to reach Reynolds numbers up to the order of 10^8, with the corresponding swirl numbers up to the order of 100. We first present the results for $W_0 = 0$, and then for $W_0 \neq 0$. In the latter case, the onset of absolute instabilities will also be characterized (no absolute instabilities are found for viscous modes with $q \geqslant 1.5$ when $W_0 = 0$).

2. Formulation of the problem and numerical method

2.1. *General basic flow and spatial stability formulation*

Although we shall consider only the spatial stability of the q-vortex (1.1), we formulate here the problem for a general vortex with axial flow which, in cylindrical-polar coordinates (r, θ, z), and in the parallel-flow approximation, has a velocity and pressure fields given by

$$U = 0, \quad V = V(r), \quad W = W(r), \quad P = P(r). \quad (2.1)$$

All the magnitudes are dimensionless. The flow is characterized by two non-dimensionl parameters: a Reynolds number

$$Re = \frac{r_c W_c}{\nu}, \quad (2.2)$$

where r_c and W_c are a characteristic radius (the dispersion radius of vorticity) and a characteristic axial velocity, respectively, and ν is the kinematic viscosity; and a swirl

parameter,

$$S_w = \frac{V_c}{W_c},\tag{2.3}$$

where V_c is a characteristic azimuthal velocity. In the case of the Batchelor's vortex (1.1), $S_w \equiv q$.

To analyse the linear stability of the above basic flow, the velocity (u, v, w) and pressure p fields, are decomposed, as usual, into their mean parts (2.1), and small perturbations (u', v', w', p'). These perturbations are decomposed in the standard form:

$$s \equiv [u', v', w', p']^T = S \, e^{az+i(n\theta-\omega t)},\tag{2.4}$$

where the complex amplitude,

$$S(r) \equiv \begin{pmatrix} F(r) \\ G(r) \\ H(r) \\ \Pi(r) \end{pmatrix},\tag{2.5}$$

depends only on the radial coordinate in the parallel-flow approximation. The non-dimensional order-of-unity complex radial wavenumber a is defined as

$$a \equiv \gamma + i\alpha.\tag{2.6}$$

The real part γ is the exponential growth rate, and the imaginary part α is the axial wavenumber. A non-dimensional frequency ω has also been defined. Finally, the azimuthal wavenumber n is equal to zero for axisymmetric perturbations, and different from zero for non-axisymmetric perturbations.

Substituting (2.4)–(2.5) into the incompressible Navier–Stokes equations, and neglecting second-order terms in the small perturbations, the following set of linear stability equations results:

$$\boldsymbol{L} \cdot \boldsymbol{S} = 0,\tag{2.7}$$

$$\boldsymbol{L} = \boldsymbol{L}_1 + a\boldsymbol{L}_2 + \frac{1}{Re}\boldsymbol{L}_3 + \frac{a^2}{Re}\boldsymbol{L}_4,\tag{2.8}$$

$$\boldsymbol{L}_1 = \begin{pmatrix} \dfrac{\mathrm{d}}{\mathrm{d}r} + \dfrac{1}{r} & i\dfrac{n}{r} & 0 & 0 \\[2mm] i\left(\dfrac{nV}{r} - \omega\right) & -\dfrac{2V}{r} & 0 & \dfrac{\mathrm{d}}{\mathrm{d}r} \\[2mm] \dfrac{\mathrm{d}V}{\mathrm{d}r} + \dfrac{V}{r} & i\left(\dfrac{nV}{r} - \omega\right) & 0 & i\dfrac{n}{r} \\[2mm] \dfrac{\mathrm{d}W}{\mathrm{d}r} & 0 & i\left(\dfrac{nV}{r} - \omega\right) & 0 \end{pmatrix},\tag{2.9}$$

$$\boldsymbol{L}_2 = \begin{pmatrix} 0 & 0 & 1 & 0 \\ W & 0 & 0 & 0 \\ 0 & W & 0 & 0 \\ 0 & 0 & W & 1 \end{pmatrix}, \quad \boldsymbol{L}_4 = \begin{pmatrix} 0 & 0 & 0 & 0 \\ -1 & 0 & 0 & 0 \\ 0 & -1 & 0 & 0 \\ 0 & 0 & -1 & 0 \end{pmatrix},\tag{2.10}$$

$$\mathbf{L}_3 = \begin{pmatrix} 0 & 0 & 0 & 0 \\ -\mathrm{D}_r^2 + \dfrac{n^2+1}{r^2} & \mathrm{i}\dfrac{2n}{r^2} & 0 & 0 \\ -\mathrm{i}\dfrac{2n}{r^2} & -\mathrm{D}_r^2 + \dfrac{n^2+1}{r^2} & 0 & 0 \\ 0 & 0 & -\mathrm{D}_r^2 + \dfrac{n^2}{r^2} & 0 \end{pmatrix}, \qquad (2.11)$$

$$\mathrm{D}_r^2 \equiv \frac{\mathrm{d}^2}{\mathrm{d}r^2} + \frac{1}{r}\frac{\mathrm{d}}{\mathrm{d}r}. \qquad (2.12)$$

These equations have to be solved with the following boundary conditions:

$$r \to \infty, \quad F = G = H = 0; \qquad (2.13)$$

$r = 0$ (Batchelor & Gill 1962),

$$F = G = 0, \quad \mathrm{d}H/\mathrm{d}r = 0, \quad (n = 0), \qquad (2.14)$$
$$F \pm \mathrm{i}G = 0, \quad \mathrm{d}F/\mathrm{d}r = 0, \quad H = 0 \quad (n = \pm 1), \qquad (2.15)$$
$$F = G = H = 0 \quad (|n| > 1). \qquad (2.16)$$

In the spatial stability analysis that will be carried out here, for a given real frequency ω, and given the parameters Re, $S_w = q$ and n, the system (2.7)–(2.16) constitutes a nonlinear eigenvalue problem for the complex eigenvalue a. The flow is considered unstable when the disturbance grows with z; i.e. when the real part of the eigenvalue, γ, is positive (provided that the group velocity is also positive; see below).

2.2. *Numerical method*

To solve (2.7)–(2.16) numerically, S is discretized using a staggered Chebyshev spectral collocation technique developed by Khorrami (1991b), where the three velocity components and the three momentum equations are discretized at the grid collocation points, whereas the pressure and the continuity equation are enforced at the mid-grid points. This method has the advantage of eliminating the need for two artificial pressure boundary conditions at $r = 0$ and $r \to \infty$, which are not included in (2.13)–(2.16). To implement the spectral numerical method, (2.7) is discretized by expanding S in terms of a truncated Chebyshev series. The boundary conditions at infinity are applied at a truncated radial distance r_{max}, chosen large enough to ensure that the results do not depend on that truncated distance. To map the interval $0 \leqslant r \leqslant r_{max}$ into the Chebyshev polynomials domain $-1 \leqslant s \leqslant 1$, we use the transformation

$$r = c_1 \frac{1-s}{c_2 + s} \quad \text{with} \quad c_2 = 1 + \frac{2c_1}{r_{max}}, \qquad (2.17)$$

where c_1 is a constant such that approximately half of the nodes are concentrated in the interval $0 \leqslant r \leqslant c_1$. This transformation allows large values of r to be taken into account with relatively few basis functions. The domain is thus discretized in N points, N being the number of Chebyshev polynomials in which S has been expanded. With this discretization, (2.7)–(2.16) becomes an algebraic nonlinear eigenvalue problem which is solved using the linear companion matrix method described by Bridges & Morris (1984). The method consists in adding to (2.5) the eigenfunction aS, obtaining thus a linear eigenvalue problem, but at the price of doubling the size of the original nonlinear one. The resulting (complex) linear eigenvalue problem is solved with double precision using an eigenvalue solver from the IMSL library (subroutine DGVCCG), which provides the entire eigenvalue and eigenvector spectrum. Spurious eigenvalues

N	$a = \gamma + i\alpha$	$k = k_r + ik_i$ (OS)
40	$0.222 + 0.365i$	
60	$0.2229717 + 0.365176287i$	$0.367202058 - 0.220458484i$
70		$0.367202508 - 0.220457875i$
80	$0.222971712 + 0.3651762873i$	$0.367202981 - 0.220457371i$
100	$0.22297171238 + 0.365176287330i$	$0.367203916 - 0.220456594i$
120	$0.2229717123848892 + 0.3651762873306434i$	

TABLE 1. Convergence behaviour of $a = \gamma + i\alpha$ for the most unstable mode with $n = -1$ and $\omega = -0.15$ for $Re = 667$, $q = 0.7$, $W_0 = 0$, as a function of the number N of Chebyshev polynomials. $c_1 = 3$, $r_{max} = 100$. Also shown are the results of Olendraru & Sellier (2002) for the same case (OS).

were discarded by comparing the computed spectra for an increasing number N of collocation points. A first selection of physical modes is made by discarding all the eigenvalues corresponding to eigenfunctions that do not die conveniently as $r \to \infty$; that is, we consider only those eigenfunctions satisfying

$$\frac{\sum_{i=1}^{N/10} |F(r_i)|^2}{\sum_{i=1}^{N} |F(r_i)|^2} < T, \tag{2.18}$$

where the r_i are the radial nodes and T is a given tolerance.

2.3. *Convergence tests*

To check the efficiency and accuracy of the numerical method, we present convergence histories for two cases. The first one (table 1) is an inviscid mode already documented in the spatial stability analysis by Olendraru & Sellier (2002, see their table 1), corresponding to $Re = 667$ and $q = 0.7$, for the azimuthal wavenumber $n = -1$ and frequency $\omega = -0.15$, obtained with the same numerical parameters ($c_1 = 3$ and $r_{max} = 100$) as those of Olendraru & Sellier (2002). It is observed that the eigenvalue is obtained with 10 significant digits for $N = 100$ collocation points (for α), and with 12 significant digits for $N = 120$. In the notation of Olendraru & Sellier (2002), the complex wavenumber k is related to our complex eigenvalue a through $a = ik$; i.e. $-k_i = \gamma$ is the growth rate, and $k_r = \alpha$ is the axial wavenumber. The convergence of the numerical results Olendraru & Sellier (2002) is less good than in our results (5 significant figures for $N = 100$), and only the two first significant digits coincide with our results. This is probably due to the differences in the eigenvalue solvers and in the machine precisions used. In any case, the coincidence in two significant figures with Olendraru & Sellier (2002) and the excellent convergence history as N increases, make us confident of our numerical results.

For the viscous modes with large q ($\geqslant 1.5$) and Re of interest here, more precision is required because the eigenfunctions are more involved. In addition, they are centre modes, concentrated near the vortex axis (see figure 1). For these reasons, we have used in the computations $N = 140$ and $c_1 = 1$, while maintaining $r_{max} = 100$. For very high Reynolds numbers ($Re \geqslant 10^7$), we have concentrated the nodes near the axis even more, using a factor $c_1 = 0.1$ (see figure 1b). For the highest Reynolds number considered, $Re = 10^8$, we have used $N = 180$, together with $c_1 = 0.1$ and $r_{max} = 100$. The second convergence history presented here (table 2) is for this last Reynolds number, $Re = 10^8$, with $q = 3$, $\omega = -2.75$, $W_0 = 0$ and $n = -1$. Note that
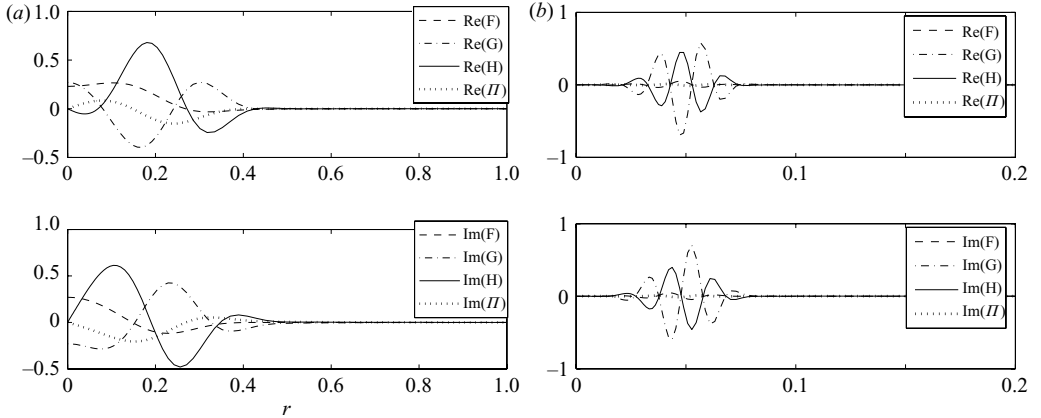
FIGURE 1. Real (Re) and imaginary (Im) parts of the eigenfuctions for (a) $Re = 10^4$, $q = 3$, $W_0 = 0$, $n = -1$, $\omega = -2.75$ ($N = 140$, $c_1 = 1$), and (b) $Re = 10^8$, $q = 3$, $W_0 = 0$, $n = -1$, $\omega = -2.75$ ($N = 180$, $c_1 = 0.1$).

N	$a = \gamma + i\alpha$
160	$1.69 \times 10^{-3} + 0.246667i$
180	$1.69658 \times 10^{-3} + 0.246667i$
200	$1.6967876 \times 10^{-3} + 0.24666715i$

TABLE 2. Convergence behaviour of $a = \gamma + i\alpha$ of the most unstable mode with $n = -1$ and $\omega = -2.75$ for $Re = 10^8$, $q = 3$, $W_0 = 0$, as a function of the number N of Chebyshev polynomials. $c_1 = 0.1$, $r_{max} = 100$.

the eigenvalue is obtained with at least 6 significant digits when $N = 180$ is used. Finally, to discard the spurious modes, a tolerance $T = 10^{-11}$ in (2.18) was used in all the reported cases.

3. Results

For real values of the frequency ω (spatial analysis), the governing stability equations have the symmetry property $a(\omega; n; Re, q) \mapsto a^*(-\omega; -n; Re, q)$, where the asterisk indicates the complex conjugate. Thus, if we allow for both positive and negative values of the forcing frequency ω, only the cases with non-positive (or non-negative) azimuthal wavenumber n have to be considered. It will be assumed that $n \leqslant 0$ in what follows. A spatial mode with $\omega < 0$, $n < 0$, and the eigenvalue $a = \gamma + i\alpha$ (for given values of Re and q), physically corresponds to a spatial mode with the positive frequency $-\omega$, the positive azimuthal wavenumber $-n$, the axial wavenumber $-\alpha$, and the same spatial growth rate γ. On the other hand, only positive values of the swirl parameter q will be considered, for the spatial stability equations are invariant under the transformation $(n, q) \rightarrow (-n, -q)$, $(F, G, H, \Pi) \rightarrow (F, -G, H, \Pi)$ (see, e.g. Olendraru & Sellier 2002). Thus, the stability properties of a vortex with swirl parameter $-q$ ($q > 0$), for azimuthal number n ($n \leqslant 0$), and any frequency ω (positive or negative) are the same as those for a vortex with q, $-n$ and ω; i.e. the same as for q, n and $-\omega$.

For $q \geqslant 1.5$ and given values of the parameters, we shall look for the least stable, or the most unstable, spatial modes propagating towards increasing z. That is, for
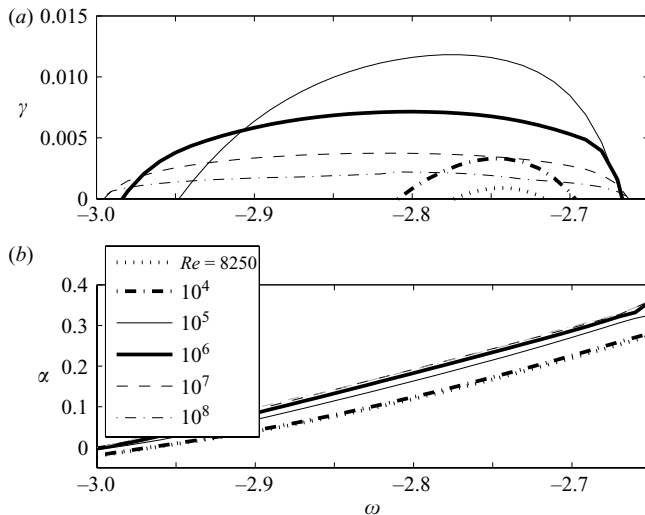
FIGURE 2. (a) $\gamma(\omega)$, and (b) $\alpha(\omega)$ for the less stable viscous modes for $q = 3$, $W_0 = 0$, $n = -1$, and different values of Re, as indicated.

each $q \geqslant 1.5$, $Re > 0$, $n \leqslant 0$, and a given positive, negative or zero value of ω, we search for the largest value of γ corresponding to a mode with a positive real part of the group velocity, which in its dimensionless form is given by

$$c_g \equiv \frac{\partial \omega}{\partial \alpha}. \qquad (3.1)$$

If $\gamma < 0$ ($\gamma > 0$), the amplitude of the wave packet corresponding to the selected forcing frequency ω, which moves downstream at the real group velocity $c_g > 0$, will decrease (increase) with z, and the flow will be spatially stable (unstable). Thus, a spatial growth rate $\gamma > 0$ with $c_g > 0$ corresponds to a convectively unstable flow, since the growing perturbation is advected downstream of the source with the forcing frequency ω, leaving the flow in its undisturbed state when the forcing ceases (see, e.g. Huerre & Monkewitz 1990).

Here, we characterize the viscous unstable modes previously found by Fabre & Jacquin (2004) for $W_0 = 0$ (for large q and large Re), but using the present spatial stability formulation instead of a temporal one, and for different values of W_0, which is now a relevant parameter in the spatial stability analysis. In particular, we shall consider only swirl numbers $q \geqslant 1.5$, so that all unstable modes (if any) are necessarily viscous modes (Lessen *et al.* 1974). In fact, we find that at most only one viscous mode may become unstable in all the cases considered for $q > 1.5$.

3.1. *Viscous modes for $W_0 = 0$ (convective instabilities)*

We start with the case $W_0 = 0$. Thus, for instance, figure 2 shows the dispersion relations, $\gamma(\omega)$ and $\alpha(\omega)$, for the unstable viscous modes with azimuthal wavenumber $n = -1$, corresponding to $q = 3$ and different Reynolds numbers. They become unstable at $Re_c \simeq 8200$ for $\omega_c \simeq -2.75$, and remain unstable for $R > Re_c$, though they become neutrally stable as $Re \to \infty$ because they are viscous modes (note that the growth rate γ first increases with Re, reaches a maximum at about $Re \approx 10^5$, and then decreases very slowly as $Re \to \infty$). The functions $\alpha(\omega)$ are always almost linear functions, so that the phase speeds $c = \omega/\alpha$ practically coincide with their group
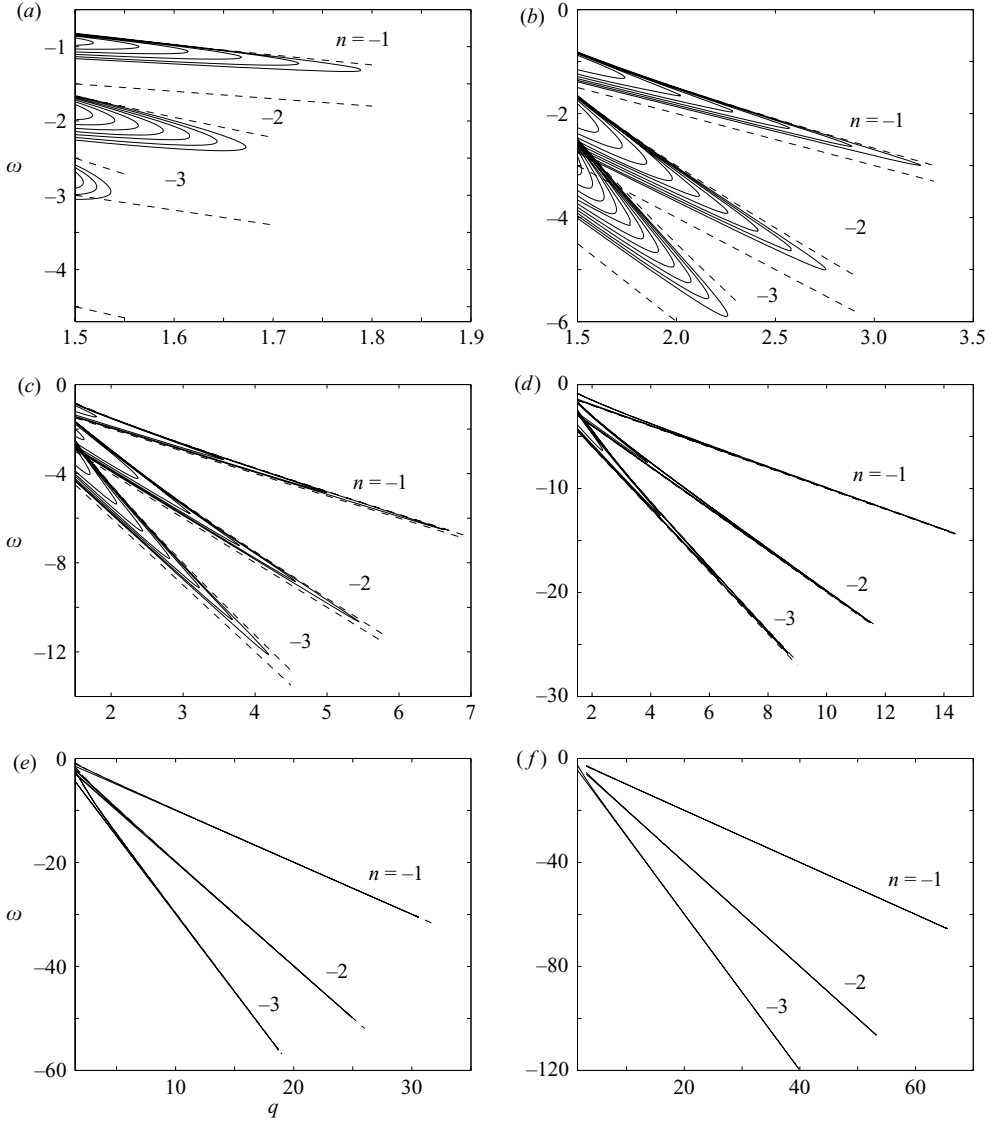
FIGURE 3. Regions of instability in the (ω, q)-plane for the most unstable mode with $n = -1$, $n = -2$ and $n = -3$ for different values of Re: (a) 10^3, (b) 10^4, (c) 10^5, (d) 10^6, (e) 10^7, (f) 10^8. The outermost continuous lines correspond to $\gamma = 0$ (neutral curves), within which we have plotted contour lines for $\gamma > 0$ (the increment in γ is 0.005 in all the cases plotted). The dashed lines correspond to the asymptotic approximation for large Re of the upper and lower neutral curves given by Le Dizès & Fabre (2007).

speeds $c_g = \partial\omega/\partial\alpha$, being both obviously positive (we look only for eigenvalues with $c_g \geqslant 0$). These features are common for all the values of $q \geqslant 1.5$ (viscous modes). Thus, no absolutely unstable modes are found, for c_g never vanishes for these viscous modes in all the cases considered here with $W_0 = 0$.

The instability regions in the (ω, q)-plane for the viscous modes with $n = -1$, -2 and -3 are summarized in figure 3 for different (high) values of the Reynolds number. For the present case with $W_0 = 0$, these viscous modes with $q > 1.5$ were not
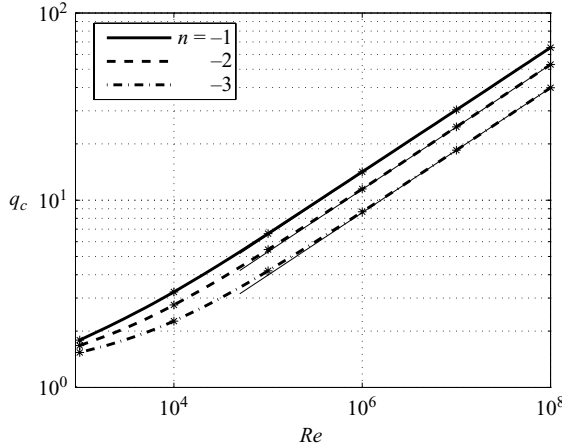
FIGURE 4. Critical swirl number above which no unstable viscous modes exist as a function of Re for several values of n. The thin continuous lines correspond to the asymptotic results (Fabre & Le Dizès 2007): $q_c/Re^{1/3} \simeq 0.1408$ for $n = -1$, 0.1142 for $n = -2$ and 0.0858 for $n = -3$.

reported in the spatial stability analysis of Olendraru & Sellier (2002). They are the spatial counterparts of the temporal viscous modes found by Fabre & Jacquin (2004), though these authors mapped the unstable region up to $Re \approx 10^6$, and we report here results up to $Re = 10^8$. For each Reynolds number and n, there exists a critical swirl number, $q_c^n(Re)$, above which the flow is stable. For instance, for $Re = 10^4$, we find that $q_c^{n=-1} \simeq 3.233$, that practically coincides with the value 3.235 reported by Fabre & Jacquin (2004). This critical swirl number is plotted as a function of the Reynolds number in figure 4 for $n = -1, -2$ and -3.

It is worth noting in figure 3 that the instability regions narrow as the Reynolds number increases, contracting to a very slender region around the straight line $\omega = nq$ for $Re \to \infty$, in accordance with the lowest order of the asymptotic results for large Reynolds numbers given by Le Dizès & Fabre (2007). These asymptotic results were a useful initial guide to finding out the frequency regions in which the present viscous modes were unstable for each q. We have include in figure 3 the asymptotic approximation to the upper and lower branches of the neutral curves. For the present q-vortex (1.1), and up to the order of $Re^{-1/2}$, the upper and lower parts of the neutral curve (for $q \geqslant 1.5$ and $n \leqslant 0$) are given by (Le Dizès & Fabre 2007)

$$\omega \sim nq + \alpha(1 + W_0) - \frac{Re^{-1/2}}{2}\sqrt{3n(2/q - q)}, \qquad (3.2)$$

with

$$\alpha \sim -n/q, \qquad (3.3)$$

for the upper branch of the neutral curve, and

$$\alpha \sim 0, \qquad (3.4)$$

for the lower branch. The dashed lines in figure 3 are given by (3.2) with $W_0 = 0$. Though these asymptotic expressions are obtained by Le Dizès & Fabre (2007) from a temporal stability analysis, the present neutral curve of the spatial stability analysis is easily found by setting to zero the imaginary part of the frequency (the growth rate),
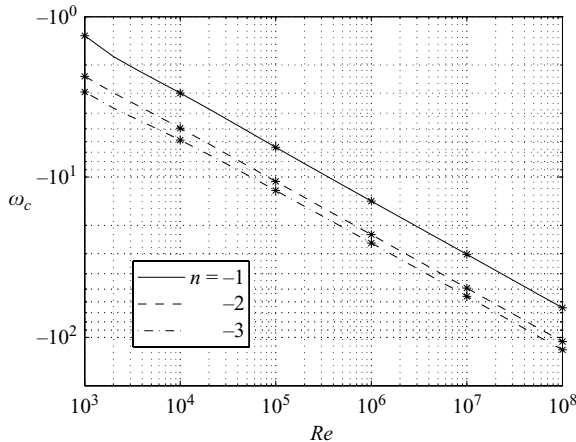
FIGURE 5. Frequencies corresponding to the critical swirl numbers plotted in figure 4.

yielding the axial wavenumber (3.3) or (3.4), and the corresponding real frequency
(3.2). The agreement between asymptotic and numerical results obviously improves
as Re increases. Thus, it is very good for $Re \geqslant 10^5$, approximately, but it is poor for
$Re = 10^3$, especially for the lowest branch of the neutral curve.

As mentioned above, figure 4 depicts the critical (maximum) swirl numbers as
functions of the Reynolds number. These values practically coincide with those
plotted in figure 3 of Fabre & Jacquin (2004) (up to $Re = 10^5$). The corresponding
frequencies are plotted in figure 5. For each Re, the largest critical swirl number
corresponds always to the helical mode with $n = -1$. It is observed that both q_c and
$|\omega_c|$ scale as $Re^{1/3}$ for large Re, as predicted by the asymptotic analysis. We have
included in figure 4 these asymptotic results for q_c (Fabre & Le Dizès 2007).

Finally, to close this section, it is important to mention that no unstable
axisymmetric ($n = 0$) viscous modes were found for $q \geqslant 1.5$.

3.2. *Viscous modes and the onset of absolute instabilities for $W_0 \neq 0$*

We consider now the viscous unstable modes when an uniform axial flow is present
in the vortex, $W_0 \neq 0$. Particularly, we pay special attention to wake-like vortices with
$W_0 < 0$, for which, as we shall see, absolute instabilities may be present in the flow
(as previously found by Delbende, Chomaz & Huerre 1998 for inviscid modes with
$q < 1.5$, and hinted for viscous modes for $Re = 10^4$ by Olendraru & Sellier 2002). We
also consider the cases with $W_0 > 0$, but they never become absolutely unstable.

Figure 6 shows the instability regions in the (ω, q)-plane for the viscous modes
($q > 1.5$) with $n = -1$, $Re = 10^3$, and different values of W_0 ranging between -1.25
and $+0.25$. It is observed that the critical (maximum) swirl number coincides for all
the values of W_0, $q_c^{n=-1}(Re = 10^3) \simeq 1.788$. This is because the temporal stability
analysis, contrary to the present spatial analysis, does not depend on W_0, so that the
stability boundary in the parameter plane (q, Re) (depicted in figure 4) is common
for all the values of W_0, for given values of n.

Inside the instability regions depicted in figure 6, flows with $W_0 \neq 0$ may
become absolutely unstable below some critical swirl number. To find these absolute
instabilities, we look for saddle points in the dispersion relation, with a cusp point in
the spatial growth rate $\gamma(\omega) > 0$ (e.g. Fernandez-Feria & del Pino 2002), and apply
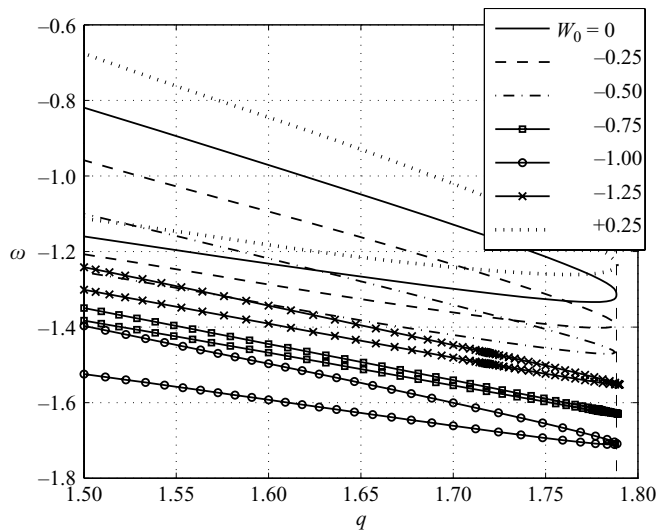the Briggs–Bers criterion (see, e.g. Huerre & Monkewitz 1990). To that end, we look

FIGURE 6. Regions of instability (neutral curves, $\gamma = 0$) in the (ω, q)-plane for the most unstable mode with $n = -1$ for $Re = 10^3$, and for different values of W_0, as indicated.
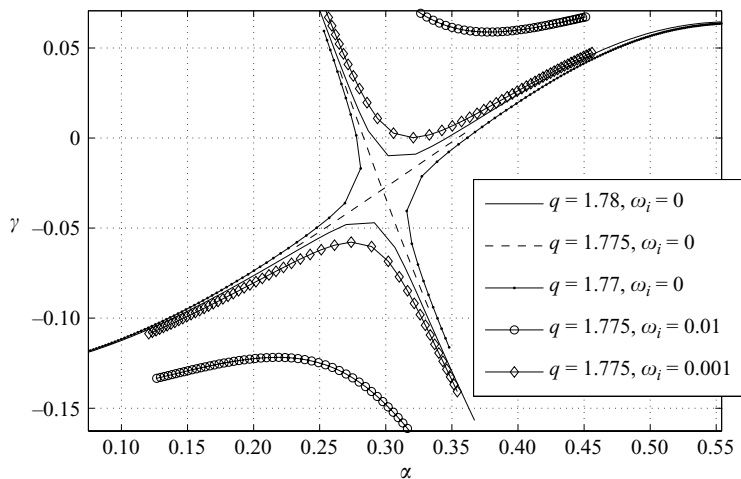

FIGURE 7. Saddle point in the dispersion relation for the case $Re = 10^3$, $n = -1$, $W_0 = -1$, which corresponds to an absolute instability for $q = q_{ca} \simeq 1.775$ and $\omega = \omega_0 \simeq -1.6151$.

for the dispersion relation functions $[\gamma(\omega), \alpha(\omega)]$ for diminishing values of q, starting from $q = q_c$. For the cases depicted in figure 6, we have found absolute instabilities for $W_0 = -0.75$ and for $W_0 = -1.0$. For instance, for $W_0 = -1$, the saddle point in the dispersion relation is shown in figure 7, which corresponds to an absolute critical swirl $q_{ca} \simeq 1.775$, and an absolute frequency $\omega_0 \simeq -1.6151$. These critical values are marked with an asterisk inside the convective instability regions in figure 8 for $W_0 = -0.75$ and $W_0 = -1$. For $q_{ca} < q < q_c$, the flow is just convectively unstable (in the frequency range inside the curves depicted in figure 8), whereas for $q < q_{ca}$, the flow may be absolutely unstable in a frequency range which obviously lies inside the convectively unstable range. We have plotted in figure 8 only the neutral curve for convective instability and the line with the maximum growth rate until it ends at
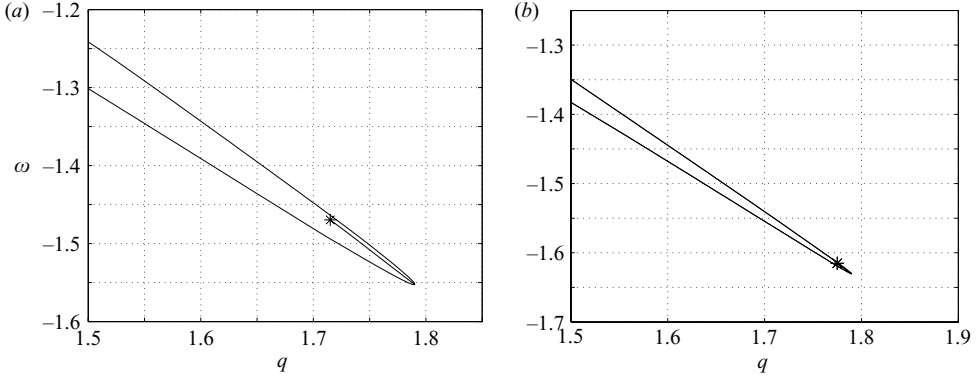
FIGURE 8. Regions of instability (neutral curves, $\gamma = 0$) in the (ω, q)-plane for the most unstable mode with $n = -1$ for $Re = 10^3$, and (a) $W_0 = -0.75$ and (b) -1. The asterisks inside the curves mark the frequency (ω_0) and swirl parameter (q_{ca}) for the onset of absolute instability (the lines ending at the asterisks correspond to the maximum growth rate for convective instabilities).
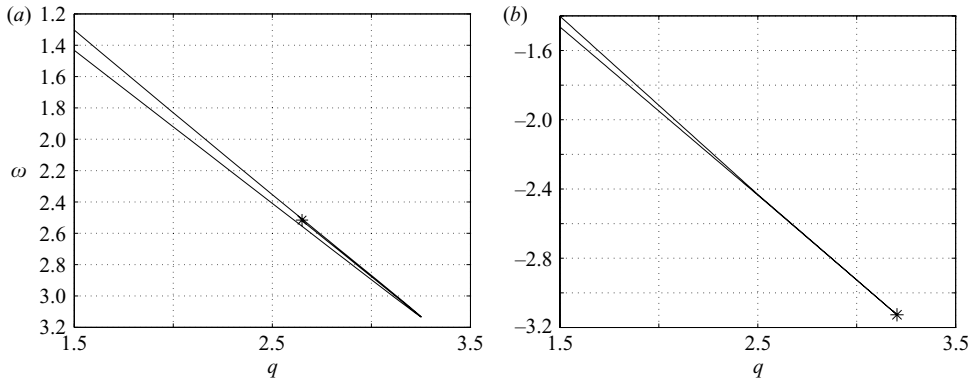

FIGURE 9. As in figure 8, but for $Re = 10^4$.

the asterisk marking the onset of absolute instability, corresponding to q_{ca} and the absolute frequency ω_0.

The analysis has been carried out for other values of Re and n. For instance, figure 9 shows the convective instability regions, and the values of q_{ca} and ω_0, for $n = -1$, $Re = 10^4$ and a couple of values of W_0. It is seen that q_{ca} approaches q_c as the Reynolds number increases for $W_0 = -1$. All the values of q_{ca} and ω_0 are plotted in figure 10 as functions of W_0 for $n = -1$ and several values of Re up to 10^6. Figure 10(a) marks, in fact, the absolutely unstable regions in the plane (q, W_0) for several values of Re. It is observed that these regions increase appreciably in size, reaching higher values of the swirl number, as Re increases. For $Re = 10^4$ practically coincides with the region depicted in figure 24 of Olendraru & Sellier (2002), with a maximum value of the swirl number $q_{ca,max}(Re = 10^4, n = -1) \simeq 3.23$. This maximum value of the critical swirl for absolute instability is always reached for $W_0 \simeq -1$, independently of Re ($W_0 = -1$ marks the boundary between co-flowing and counter-flowing wakes). Thus, Batchelor's vortex wakes with $W_0 = -1$ are the globally most unstable members of the family of vortices. This is easy to understand since, in
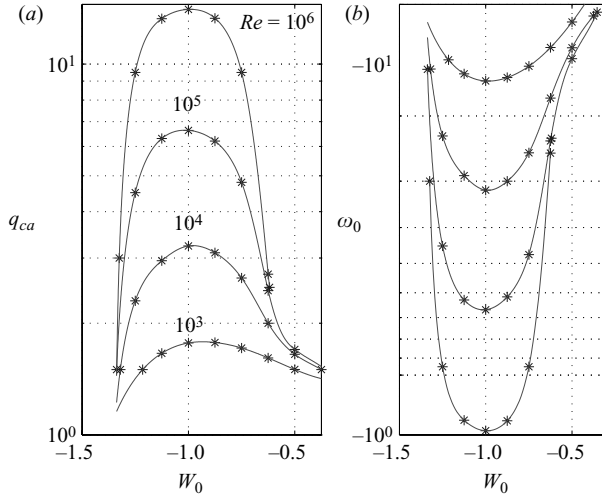
FIGURE 10. (a) q_{ca}, and (b) ω_0 as functions of W_0 for $n = -1$ and several values of Re (as indicated).
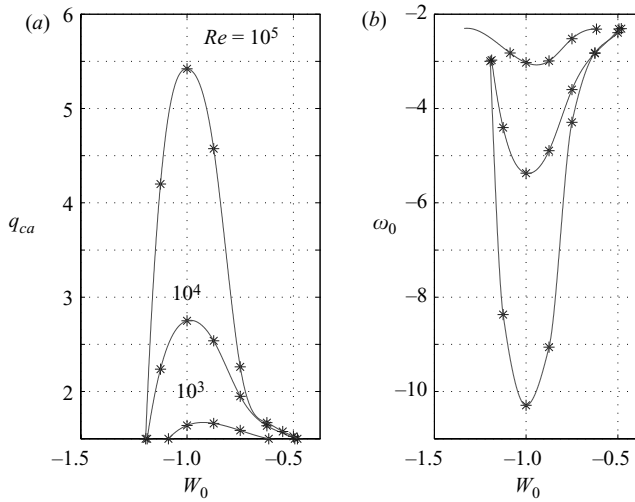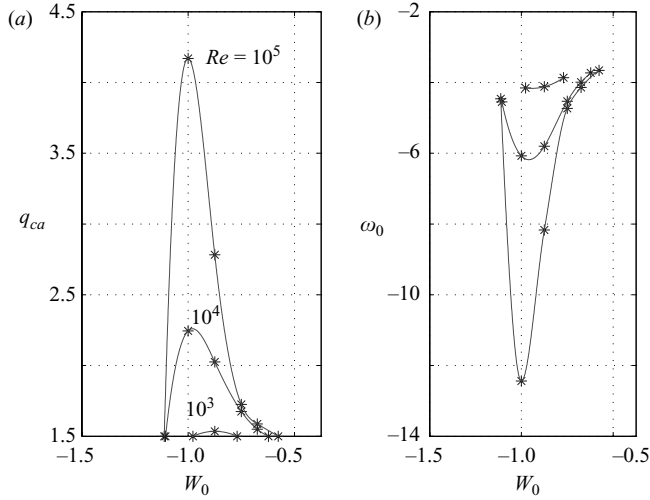

FIGURE 11. As in figure 10, but for $n = -2$.

this case, the vortex centre is a stagnant region, and the instabilities considered here are localized in this region.

Figures 11 and 12 show the critical values for absolute instabilities for modes with azimuthal wavenumbers $n = -2$ and $n = -3$ as functions of W_0. The maximum values of q_{ca} for each Re are also reached at $W_0 \simeq -1$, as in the $n = -1$ case, except for the lower Reynolds number considered ($Re = 10^3$) in the case $n = -3$ (see figure 12). All the maximum values of q_{ca} as functions of Re are plotted in figure 13 for $n = -1, -2$ and -3. As in the case of convective instabilities, helical waves with $n = -1$ are those with the largest region of absolute instability for Batchelor's vortices. It is observed that, for large Re, $q_{ca,max}$ scales as $Re^{1/3}$. In fact, as seen in figure 8 for $Re = 10^4$, q_c and q_{ca} almost coincide for large Re when $W_0 = -1$, so that this asymptote coincides with that shown in figure 4, and with the asymptotic results of Fabre & Le Dizès

FIGURE 12. As in figure 10, but for $n = -3$.
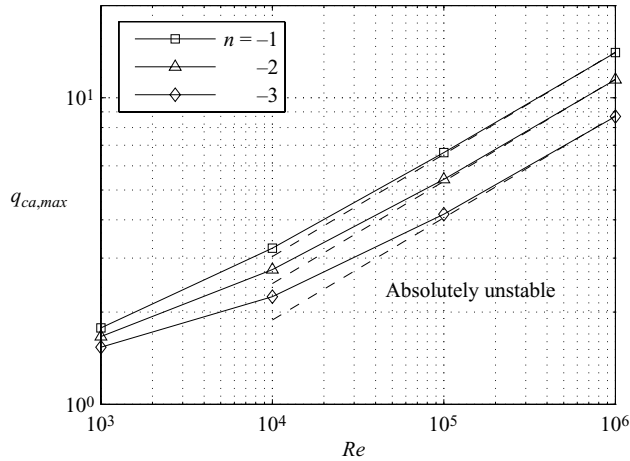
FIGURE 13. $q_{ca,max}$ as a function of Re for the three values of n considered. For large Re, these curves behave as $q_{ca,max} \simeq c_n Re^{1/3}$ (dashed lines), with the constants c_n for each $-n$ approximately equal to those given in the caption of figure 4.

(2007). This could have been anticipated because whenever the flow is unstable, there is one reference frame, which in this problem corresponds to one value of W_0 ($= -1$ in this case), in which the instability is absolute. Finally, figure 14 shows q_{ca} as a function of Re for the three values of n considered and for $W_0 = -1.125$, and -0.75 (the case $W_0 = -1$ is not included because it coincides with figure 13, except for the point corresponding to $Re = 10^3$ for $n = -3$). In the case $W_0 = -1.125$, no curve for $n = -3$ is given because the flow is not absolutely unstable for this W_0 for any value of Re (see figure 12). For large Re, q_{ca} scales as $Re^{1/3}$, similarly to the case $W_0 = -1$, with proportionality constants given in the figure caption. This type of asymptotic behaviour for large Re is also found for the case $W_0 = -0.75$, but only for $n = -1$. For $n = -2$ and $n = -3$, the values of q_{ca} are now low and so close to the viscous
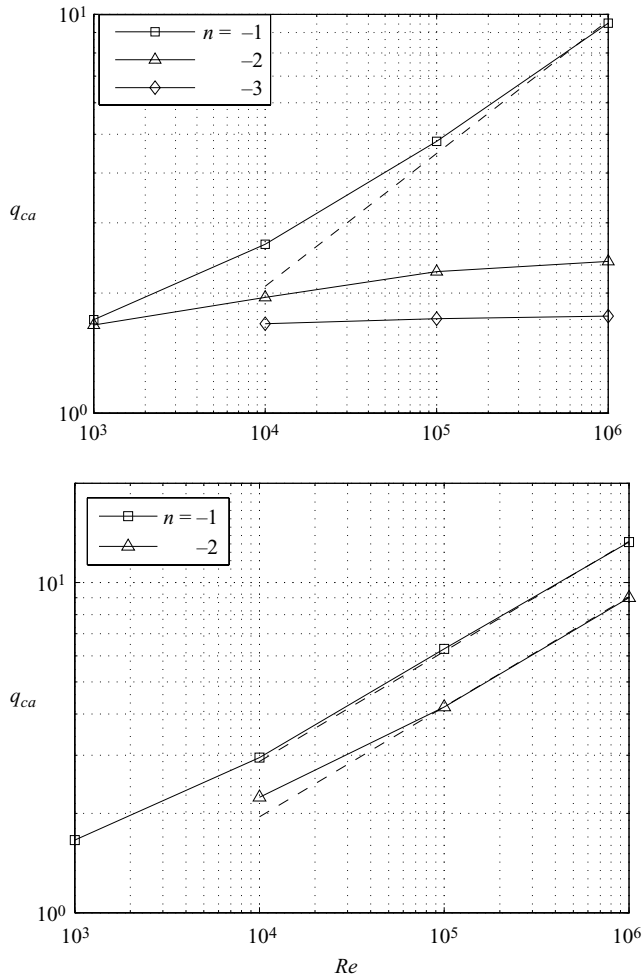
FIGURE 14. q_{ca} as a function of Re for $n = -1, -2$ and -3, and for (*a*) $W_0 = -0.75$ and (*b*) $W_0 = -1.125$. With dashed lines, we show the asymptotic behaviours for large Re, $q_{ca} \simeq c_n Re^{1/3}$, if that is the case: $c_1 \simeq 0.0965$ for $W_0 = -0.75$; $c_1 \simeq 0.1333$ and $c_2 \simeq 0.0906$ for $W_0 = -1.125$.

instability boundary $q \approx 1.5$ that the asymptotic behaviour for the viscous centre modes discussed by Le Dizès & Fabre (2007) is no longer valid.

4. Summary and conclusions

We have characterized the viscous instabilities of Batchelor's vortex for high swirl numbers. In particular, we have considered $q > 1.5$, a range of the swirl parameter in which Batchelor's vortex does not present inertial instabilities (Mayer & Powell 1992). These viscous instabilities, which are centre modes concentrated near the axis of the vortex, were found by Fabre & Jacquin (2004) using a temporal stability analysis. Here, we use a spatial stability analysis which, although it is numerically more involved, since one has to tackle a nonlinear eigenvalue problem, has the advantage of directly providing relevant physical information such as the frequency ranges of the unstable modes in terms of the other parameters of the flow, namely the Reynolds

number and the swirl parameter, and in terms of the azimuthal wavenumber of the perturbations. It also provides the onset of absolute instability in a straightforward way.

We have fully characterized the convective viscous instabilities from $Re = 10^3$, which is approximately the lowest Reynolds number for which the viscous instabilities for large q (> 1.5) do appear, up to the remarkably high value $Re = 10^8$. For these very high Reynolds numbers we find excellent agreement with the asymptotic analysis of Le Dizès & Fabre (2007). We find that the most unstable modes are helical ones with azimuthal wavenumber $n = -1$. The critical, or maximum, swirl number for convective instability scales as $Re^{1/3}$ for large Re, as predicted by the asymptotic analysis (Le Dizès & Fabre 2007). No axisymmetric ($n = 0$) unstable viscous modes are found.

We also characterize the absolute/convective instability boundary for these viscous modes. Again, helical modes with $n = -1$ are the first to become absolutely unstable as q decreases, for each Re. Absolute instabilities are present only when the uniform axial velocity superimposed to the vortex, W_0, is negative, i.e. for wakes. In particular, the case $W_0 = -1$, which corresponds to the axial velocity that marks the boundary between co-flowing and counter-flowing wakes, is always the most absolutely unstable one for every Re and n, as could have been anticipated because, in this case, the vortex centre, where the present instabilities are localized, is a stagnant region. For large Re, the maximum swirl number for absolute instability (occurring for $W_0 = -1$) also scales as $Re^{1/3}$. Actually, we show that, for this case $W_0 = -1$, the critical swirls for convective and absolute instabilities practically coincide.

REFERENCES

Ash, R. L. & Khorrami, M. R. 1995 Vortex stability. In *Fluid Vortices* (ed. S. I. Green), chap. 8, pp. 317–372. Kluwer.

Batchelor, G. K. 1964 Axial flow in trailing line vortices. *J. Fluid Mech.* **20**, 645–658.

Batchelor, G. K. & Gill, A. E. 1962 Analysis of the stability of axisymmetric jets. *J. Fluid Mech.* **14**, 529–551.

Bridges, T. J. & Morris, P. J. 1984 Differential eigenvalue problems in which the parameter appears nonlinearly. *J. Comput. Phys.* **55**, 437–460.

Delbende, I., Chomaz, J.-M. & Huerre, P. 1998 Absolute/convective instabilities in the Batchelor vortex: a numerical study of the linear impulse response. *J. Fluid Mech.* **355**, 229–254.

Duck, P. W. & Foster, M. R. 1980 The inviscid stability of a trailing line vortex. *Z. Angew. Math. Phys.* **31**, 524–532.

Duck, P. W. & Khorrami, M. R. 1992 A note on the effect of viscosity on the stability of a trailing line vortex. *J. Fluid Mech.* **245**, 175–189.

Fabre, D. & Jacquin, L. 2004 Viscous instabilities in trailing vortices at large swirl numbers. *J. Fluid Mech.* **500**, 239–262.

Fabre, D. & Le Dizès, S. 2007 Viscous and inviscid centre-modes in vortices: the vicinity of the neutral curves. *J. Fluid Mech.* (submitted).

Fernandez-Feria, R. & del Pino, C. 2002 The onset of absolute instability of rotating Hagen–Poiseuille flow: a spatial stability analysis. *Phys. Fluids* **14**, 3087–3097.

Huerre, P. & Monkewitz, P. A. 1990 Local and global instabilities in spatially developing flows. *Annu. Rev. Fluid Mech.* **22**, 473–537.

Khorrami, M. R. 1991a On the viscous modes of instability of a trailing line vortex. *J. Fluid Mech.* **225**, 197–212.

KHORRAMI, M. R. 1991*b* A Chebyshev spectral collocation method using a staggered grid for the stability of cylindrical flows. *Intl J. Numer. Meth. Fluids* **12**, 825–833.

LE DIZÈS, S. & FABRE, D. 2007 Large-Reynolds-number asymptotic analysis of viscous centre modes in vortices. *J. Fluid Mech.* (submitted).

LEIBOVICH, S. & STEWARTSON, K. 1983 A sufficient condition for the instability of columnar vortices. *J. Fluid Mech.* **126**, 335–356.

LESSEN, M. & PAILLET, F. 1974 The stability of a trailing line vortex. Part 2. Viscous theory. *J. Fluid Mech.* **65**, 769–779.

LESSEN, M., SINGH, P. J. & PAILLET, F. 1974 The stability of a trailing line vortex. Part 1. Inviscid theory. *J. Fluid Mech.* **63**, 753–763.

MAYER, E. W. & POWELL, K. G. 1992 Viscous and inviscid instabilities of a trailing vortex. *J. Fluid Mech.* **245**, 91–114.

OLENDRARU, C. & SELLIER, A. 2002 Viscous effects in the absolute-convective instability of the Batchelor vortex. *J. Fluid Mech.* **459**, 371–396.

STEWARTSON, K. & BROWN, S. 1985 Near-neutral centre-modes as inviscid perturbations to a trailing line vortex. *J. Fluid Mech.* **156**, 387–399.

STEWARTSON, K. & CAPELL, K. 1985 On the stability of ring modes in a trailing line vortex: the lower neutral points. *J. Fluid Mech.* **156**, 369–386.

STEWARTSON, K. & LEIBOVICH, S. 1987 On the stability of a columnar vortex to disturbances with large azimuthal wavenumbers: the upper neutral points. *J. Fluid Mech.* **178**, 549–566.

STEWARTSON, K., NG, T. W. & BROWN, S. 1988 Viscous centre modes in the stability of swirling Poiseuille flow. *Phil. Trans. R. Soc. Lond.* A **324**, 473–512.